Generalized higher-order nonlinear energy operators

Fabien Salzenstein,[1] Abdel-Ouahab Boudraa,[2,*] and Jean-Christophe Cexus[2]

[1]*CNRS/Sciences et Technologies de l'Information et de la Communication-UPR 292, Université Louis Pasteur Laboratoire Iness, 23, rue du Loess, BP20 CR-67037 Strasbourg Cedex 2, France*

[2]*Institut de Recherche de l'Ecole Navale, Ecole Navale/E^{3}I^2 (EA 3876) Ecole Nationale Supérieure des Ingénieurs des Etudes et Techniques d'Armement, Lanvéoc Poulmic, BP600, 29240 Brest–Armées, France*

[*]*Corresponding author: boudra@ecole-navale.fr*

Received January 23, 2007; revised September 1, 2007; accepted September 10, 2007; posted September 28, 2007 (Doc. ID 79330); published November 19, 2007

We extend and generalize the Teager–Kaiser [in *Proceedings of IEEE International Conference on Acoustics, Speech, and Signal Processing* (1993), Vol. 3, p. 149] and the higher-order differential energy operators [IEEE Signal Process. Lett. **2**, 152 (1995)] to a large class of operators called higher-order energy operators. We show that for AM-FM signal demodulation, the introduced partial derivative orders have to satisfy certain conditions. These operators are parameterized for local processing of AM-FM signals. The operators are illustrated using synthetic signals and a real signal from light scanning interferometry. © 2007 Optical Society of America

OCIS codes: 100.0100, 260.0260.

1. INTRODUCTION

The Teager–Kaiser energy operator (TKEO) [1] is defined as a local energy measure for oscillating (simple harmonic) signals. This operator computes the energy of a real-valued signal $x(t)$ as follows:

$$\Psi[x(t)] = [x^{(1)}(t)]^2 - x^{(0)}(t)x^{(2)}(t), \tag{1}$$

where $x^{(k)}(t)$ denotes the kth derivative of $x(t)$. In the discrete case, the time derivatives are approximated by time differences. Thus, one discrete-time counterpart of the TKEO becomes [2]

$$\Psi[x(n)] = x^2(n) - x(n+1)x(n-1). \tag{2}$$

Equation (2) shows that only three samples are required for the energy estimation at each time instant. This is why the TKEO is qualified as an instantaneous energy operator. This excellent time resolution provides us with an ability to capture the signal energy fluctuations. Furthermore, this operator is very easy to implement efficiently. The TKEO has found applications in speech analysis [2], and in signal [3] and image processing [4,5]. An interesting application lies in the field of interferometry, where the luminance signals are approximated by an AM-FM monocomponent model. In this way, the extraction of the envelope or the phase provides useful information, such as the position of the surface, in order to measure the roughness of the structure. It is also possible to process the two-component signals, combining different higher-order operators [6]. For a monocomponent AM-FM signal, the TKEO is able to extract the instantaneous envelope and frequency information [2]. Maragos and Potamianos [7] have proposed an extension of the TKEO, called the k-order differential energy operator (DEO) Ψ_k, given by

$$\Psi_k[x(t)] = x^{(1)}(t)x^{(k-1)}(t) - x^{(0)}(t)x^{(k)}(t). \tag{3}$$

For $k=2$ the TKEO corresponds to the second-order differential energy operator. It is also possible to demodulate an AM-FM signal using this class of operators. A continuous version of DEO has been extended to 2D signals (images) to measure the surface shape of a material in interference microscopy [5,8].

In this work a large class of continuous DEOs is introduced. A new formulation of this continuous DEO is introduced using higher-order partial derivatives with a continuous lag parameter τ of the signal. This new family of operators leads to more flexible operators in terms of sampling rate precision and computing time. Examples of envelope and frequency detection, using the proposed operators, of a noisy synthetic signal and a real one are presented.

2. HIGHER-ORDER ENERGY OPERATORS

The higher-order energy operator (HEO), $\Psi_{p,q,m,l}[x(t)]$, is based on the four partial pth, qth, mth, and lth derivatives of a signal, $x(t)$, satisfying the condition $p+q=m+l$, $(p,q) \neq (m,l)$, and is defined as follows:

$$\Psi_{p,q,m,l}[x(t)] = x^{(p)}(t)x^{(q)}(t) - x^{(m)}(t)x^{(l)}(t). \tag{4}$$

The HEO measures the higher-order energies of a classical monocomponent harmonic oscillator (mass suspended by a spring), which is subjected to a displacement of $x(t)$, and normalized to half unit mass [7]. It is easy to see that for the derivative order combinations ($p=1$, $q=k-1$, $m=0$, $l=k$) and ($p=1$, $q=1$, $m=0$, $l=2$), the HEO is reduced to the DEO [7] and to the TKEO [1], respectively. The relations between the different orders lead to the following equations:

$$\frac{\partial \Psi_{p,q,m,l}}{\partial t}[x(t)] = \Psi_{p+1,q,m+1,l}[x(t)] + \Psi_{p,q+1,m,l+1}[x(t)],$$

$$\Psi_{p,q,m,l}[\dot{x}(t)] = \Psi_{p+1,q+1,m+1,l+1}[x(t)],$$

where $\dot{x}(t)$ represents the first derivative of the signal $x(t)$. It is possible to unify the operators into k-order operators, where $k=p+q=m+l$. To differentiate this operator from $\Psi_k[x(t)]$, we denote it $\Psi_{H_{k,p,m}}[x(t)]$. It is important to keep in mind that Ψ_k corresponds to only one operator of order k, while $\Psi_{H_{k,p,m}}$ is a set of operators of order k.

A. Discretizing the Higher-Order Energy Operator

If we replace continuous derivatives of $x(t)$ with a two-sample symmetric difference, the p-order derivative of $x(t)$ is a function of its $(p-1)$-order one,

$$x^{(p)}(nT_s) = \frac{x^{(p-1)}((n+1)T_s) - x^{(p-1)}((n-1)T_s)}{2T_s}, \tag{5}$$

where T_s is the sampling period. The system defined by this difference [Eq. (5)] is a finite impulse response (FIR) filter where the frequency response is given by

$$H(z) = \frac{z - z^{-1}}{2T_s}. \tag{6}$$

Thus, the p-order derivative can be rewritten using the binomial coefficient as follows:

$$X^{(p)}(z) = X(z)H^p(z) = X(z)\frac{1}{(2T_s)^p}\sum_{k=0}^{k=p} C_p^k(-1)^{p-k}z^k z^{k-p},$$

$$= \frac{1}{(2T_s)^p}\sum_{k=0}^{k=p} C_p^k(-1)^{p-k}z^{2k-p}. \tag{7}$$

Using the Z-inverse transform we obtain

$$x^{(p)}(n) = \frac{1}{(2T_s)^p}\sum_{k=0}^{k=p} C_p^k(-1)^{p-k}x(n+2k-p). \tag{8}$$

Thus, the quantity $Q_k[x(n)]=x^{(p)}(n)x^{(q)}(n)-x^{(m)}(n)x^{(l)}(n)$ provides

$$Q_k[x(n)] = \frac{1}{(2T_s)^k} \times \left[\sum_{i=0}^{i=p}\sum_{j=0}^{j=q} C_p^i C_q^j (-1)^{k-(i+j)} \times x(n+2i-p)x(n+2j-q) - \sum_{i=0}^{i=m}\sum_{j=0}^{j=l} C_m^i C_l^j (-1)^{k-(i+j)} \times x(n+2i-m)x(n+2j-l) \right]. \tag{9}$$

Taking the most extreme samples in the expression (9) leads to the following higher-order symmetric and discrete operator denoted by $\Psi_{H^d_{k,p,m}}$:

k even:

$$\Psi_{H^d_{k,p,m}}[x(n)] = \frac{1}{2}[x(n+p)x(n+q) + x(n-p)x(n-q) - (x(n+m)x(n+l) + x(n-m)x(n-l))], \tag{10}$$

k odd:

$$\Psi_{H^d_{k,p,m}}[x(n)] = \frac{1}{2}[x(n+m)x(n+l) + x(n-m)x(n-l) - (x(n+p)x(n+q) + x(n-p)x(n-q))]. \tag{11}$$

B. Continuous Demodulation

Consider the demodulation problem of a real AM-FM signal, $x(t)=a(t)\cos(\omega(t)t+\alpha)$, into its amplitude envelope $|a(t)|$ and instantaneous frequency (IF) $\omega(t)$. We make the assumption that $a(t)$ and $\omega(t)$ do not vary too fast (rate of change) or too greatly (range of value) with time compared to the carrier frequency of $x(t)$ [9,10]. Thus, locally, for the short time interval, $J=[t_1,t_2]$ where $(t_2-t_1)\ll T$, we can make the approximation that $a(t_0)\simeq A$ and $\omega(t_0)\simeq\Omega$, $t_0\in J$. T is the signal duration. In this case $x(t)$ is locally approximated by a pure sinusoid, $x(t)=A\cos(\Omega t+\alpha)$. It is easy to see that the pth derivative of $x(t)$ can be written as

$$x^{(p)}(t_0) = A\Omega^p \cos\left(\Omega t_0 + \alpha + \frac{\pi}{2}p\right).$$

The output of $\Psi_{H_{k,p,m}}$ for $x(t_0)$ is given by

$$\Psi_{H_{k,p,m}}[x(t_0)] = \frac{A^2\Omega^k}{2}\left[\cos\left((p-q)\frac{\pi}{2}\right) - \cos\left((m-l)\frac{\pi}{2}\right)\right]. \tag{12}$$

Using a trigonometric identity, relation (12) can be written as

$$\Psi_{H_{k,p,m}}[A\cos(\Omega t_0+\alpha)] = A^2\Omega^k \sin\left(\frac{\pi}{4}c\right)\sin\left(\frac{\pi}{4}b\right), \tag{13}$$

where

$$c = p - q + m - l = 2(m+p-k),$$

$$b = q - p + m - l = 2(m-p). \tag{14}$$

$\Psi_{H_{k,p,m}}$ output of $\dot{x}(t_0)$ is given by

$$\Psi_{H_{k,p,m}}[\dot{x}(t_0)] = \Psi_{H_{k,p,m}}[A\Omega\cos(\Omega t_0+\alpha+\pi/2)], \tag{15}$$

$$= A^2\Omega^{k+2}\sin\left(\frac{\pi}{4}c\right)\sin\left(\frac{\pi}{4}b\right). \tag{16}$$

Thus, provided that $\sin[(\pi/4)c]\sin[(\pi/4)b]\neq 0$ one can write

$$\frac{\Psi_{H_{k,p,m}}[\dot{x}(t_0)]}{\Psi_{H_{k,p,m}}[x(t_0)]} = \frac{A^2\Omega^{k+2}\sin[(\pi/4)c]\sin[(\pi/4)b]}{A^2\Omega^k\sin[(\pi/4)c]\sin[(\pi/4)b]} = \Omega^2. \tag{17}$$

Let us consider now the parameters (p_1,q_1,m_1,l_1) so that $p_1+q_1=m_1+l_1=2k$:

$$\Psi_{H_{2k,p1,m1}}[A\cos(\Omega t_0+\alpha)] = A^2\Omega^{2k}\sin\left(\frac{\pi}{4}c_1\right)\sin\left(\frac{\pi}{4}b_1\right), \tag{18}$$

where

$$c_1 = p_1 - q_1 + m_1 - l_1 = 2(m_1 + p_1 - 2k),$$

$$b_1 = q_1 - p_1 + m_1 - l_1 = 2(m_1 - p_1). \tag{19}$$

Finally, Eqs. (13) and (18) yield

$$\frac{\Psi^2_{H_{k,p,m}}[x(t_0)]}{\Psi_{H_{2k,p1,m1}}[x(t_0)]} = \frac{A^4\Omega^{2k}\sin^2[(\pi/4)c]\sin^2[(\pi/4)b]}{A^2\Omega^{2k}\sin[(\pi/4)c_1]\sin[(\pi/4)b_1]},$$

$$= A^2\frac{\sin^2[(\pi/4)c]\sin^2[(\pi/4)b]}{\sin[(\pi/4)c_1]\sin[(\pi/4)b_1]}. \tag{20}$$

According to Eq. (13) in order to estimate the product of the amplitude, A, and the IF, Ω, by $\Psi_{H_{k,p,m}}$, as for the TKEO [2], the factors $|\sin[(\pi/4)c]\sin[(\pi/4)b]|$ and $|\sin[(\pi/4)c_1]\sin[(\pi/4)b_1]|$ must approximately be equal to 1. A usual way that this can happen is when the amount of modulation is small and the bandwidths of the amplitude and the frequency modulating signals are much smaller than the carrier frequency [4]. Under these conditions, detailed in proposition 1 (see Subsection 2.E):

$$\frac{\Psi^2_{H_{k,p,m}}[x(t_0)]}{\Psi_{H_{2k,p1,m1}}[x(t_0)]} \simeq A^2. \tag{21}$$

For different short intervals $J\subset T$, Ω and A are calculated using relations (17) and (21), respectively. For an estimation of the envelope and the IF, over the interval T, of $x(t)$ the following relations are used:

$$\omega^2(t) \simeq \frac{\Psi_{H_{k,p,m}}[\dot{x}(t)]}{\Psi_{H_{k,p,m}}[x(t)]}, \tag{22}$$

$$a^2(t) \simeq \frac{\Psi^2_{H_{k,p,m}}[x(t)]}{\Psi_{H_{2k,p1,m1}}[x(t)]}. \tag{23}$$

C. Discrete Demodulation

Let a real-valued signal be $x(n)=A\cos(\Omega n+\theta)$ with $\Omega=\omega T_s$. For p and q integers we have

$$x(n+p)x(n+q) = \frac{A^2}{2}(\cos(2\Omega n+\Omega k+2\theta)+\cos(p-q)\Omega). \tag{24}$$

For k-order even, the output of $\Psi_{H_{k,p,m}}$ gives

$$\Psi_{H^d_{k,p,m}}[x(n)] = \frac{A^2}{2}(\cos(p-q)\Omega - \cos(m-l)\Omega),$$

$$= A^2\sin\left(b\frac{\Omega}{2}\right)\sin\left(c\frac{\Omega}{2}\right), \tag{25}$$

where $b=q-p+m-l$ and $c=p-q+m-l$. Since

$$b = 2(m-p), \quad c = 2(m+p-k),$$

$\Psi_{H_{k,p,m}}$ applied to $x(n)$ gives

$$\Psi_{H^d_{k,p,m}}[x(n)] = A^2\sin((m-p)\Omega)\sin((m+p-k)\Omega). \tag{26}$$

In similar fashion, for k-order odd we have

$$\Psi_{H^d_{k,p,m}}[x(n)] = \frac{A^2}{2}(\cos(m-l)\Omega - \cos(p-q)\Omega), \tag{27}$$

$$= A^2\sin((p-m)\Omega)\sin((m+p-k)\Omega). \tag{28}$$

The interest of such formulation is the relative robustness of $\Psi_{H_{k,p,m}}$ against noise. Indeed, contrary to the continuous version [Eq. (13)], in the discrete version [Eqs. (26) or (28)] there is no multiplicative frequency term, Ω^k. This frequency factor may contain some high-frequency components of the noise. If we replace the derivative of $x(t)$ with backward difference, $x_1(n)=x(n)-x(n-1)$, we obtain

$$x_1(n) \simeq A[\cos(\Omega n+\theta) - \cos(\Omega(n-1)+\theta)], \tag{29}$$

$$= -2A\sin(\Omega/2)\sin(\Omega(n-0.5)+\theta). \tag{30}$$

$\Psi_{H_{k,p,m}}$ (k even) applied to $x_1(n)$ gives

$$\Psi_{H^d_{k,p,m}}[x_1(n)] = 4A^2\sin^2\left(\frac{\Omega}{2}\right)\sin\left(b\frac{\Omega}{2}\right)\sin\left(c\frac{\Omega}{2}\right). \tag{31}$$

If $\sin(\Omega/2)\simeq\Omega/2$ then

$$\Psi_{H^d_{k,p,m}}[x_1(n)] \simeq A^2\Omega^2\sin\left(b\frac{\Omega}{2}\right)\sin\left(c\frac{\Omega}{2}\right). \tag{32}$$

Finally, for discrete $\Psi_{H_{k,p,m}}$, estimation of envelopes and IFs is given by relations (33) and (34):

$$\hat{\Omega}^2 = \frac{\Psi_{H^d_{k,p,m}}[x_1(n)]}{\Psi_{H^d_{k,p,m}}[x(n)]}, \tag{33}$$

$$\hat{A} = \sqrt{\frac{\Psi_{H^d_{k,p,m}}[x(n)]}{\sin[(m-p)\Omega]\sin[(m+p-k)\Omega]}}. \tag{34}$$

In this work we compare the discrete operators $\Psi_{H_{k,p,m}}$ [Eq. (10)] with those of Maragos and Potamianos [7]:

$$\Phi_{km}[x(n)] = x(n)x(n+k) - x(n-m)x(n+m+k). \tag{35}$$

For carrier frequency small compared to the T_s, estimation of envelopes and IFs by Φ_{km} is given by relations (36) and (37):

$$\hat{\Omega}^2 = \frac{\Phi_{km}[x_1(n)]}{\Phi_{km}[x(n)]}, \tag{36}$$

$$\hat{A} = \sqrt{\frac{\Phi_{km}[x(n)]}{\sin(m\Omega)\sin((m+k)\Omega)}}. \tag{37}$$

Note that for the operator [Eq. (35)], values $k=0$ and $m=1$ give the TKEO. Comparative study of operators given by Eq. (35) has been done in [4]. Only the most efficient operators corresponding to $(k,m)=(0,1)$ and $(k,m)=(2,1)$ are studied in this work.

D. Orders Selection of the Filters

Orders are selected such that

$$\left|\sin\left(b\frac{\Omega}{2}\right)\sin\left(c\frac{\Omega}{2}\right)\right| \simeq 1. \tag{38}$$

This condition introduces some constraints on T_s and on the integers b and c:

$$b\Omega = (2k_1+1)\pi, \quad c\Omega = (2k_2+1)\pi. \tag{39}$$

For k even we have

$$2(m-p)\Omega = (2k_1+1)\pi, \quad 2(m+p-k)\Omega = (2k_2+1)\pi. \tag{40}$$

Thus,

$$\frac{m-p}{m+p-k} = \frac{2k_1+1}{2k_2+1}. \tag{41}$$

This ratio shows that the choice of odd numerator and denominator is compatible with relation (38). Note that the k order must be even. Furthermore, since $\Psi_{H_{k,p,m}}$ is an energy operator, the quantities [Eqs. (26) and (28)] must be positive, and consequently m must be greater than p. For example, the TKEO corresponds to order 2 ($k=2$) and the associated integers are $p=q=1$, $m=2$, and $l=0$.

E. Demodulation Conditions

Let us now write the conditions for envelope and frequency detections. According to Eq. (14), in order to have the sinusoidal product of Eq. (13) equal to 1, $(m-p)$ and $(m+p-k)$ should be odd integers of the form $(m-p)=2n_1+1$ and $(m+p-k)=2n_2+1$. Thus, we find that k is an even value given by $k=2(n_1-n_2+p)$. Thus, to demodulate an AM-FM signal the orders of the continuous operators are even [10].

Proposition 1. *For a continuous k-order operator, the condition that both p and m cannot be simultaneously odd or even is necessary.*

Proof. Suppose that $m=2m_1$ and $p=2p_1$ (even integers). Since k is even, it can be written as $k=2k_1$. Thus, $(m-p)+(m+p-k)=2m-k=2n_1+2n_2+2 \Rightarrow m=k_1+n_1+n_2+1=2m_1$ and $(m+p-k)-(m-p)=2p-k=2(n_2-n_1) \Rightarrow p=n_2-n_1+k_1=2p_1$. These two relations give $2(n_2+k_1)+1=2(p_1+m_1)$, which is false. The demonstration for the odd case is obtained in a similar fashion. In conclusion, the order of these operators must be even with the condition that p and m or q and l are not odd or even at the same time. This introduces some restrictions on the choice of the operators. For example, the possible pairwise representation of $(p,q),(m,l)$ through the order 4 are

- $k=2$: $(p,q)=(2,0);(m,l)=(1,1)$.
- $k=3$: no efficient operator (odd integer).
- $k=4$: $(p,q)=(4,0);(m,l)=(3,1)$.
- $k=4$: $(p,q)=(2,2);(m,l)=(3,1)$.

Note that the order 4 gives two possibilities, instead of only one for the four-order HEO of Maragos and Potamianos [7].

F. Application to Interference Signal Demodulation

It is well-known in white light interferometry that the fringe signal looks a lot like an AM signal. When in white light emission the mean value of the wavelength is known, it is thus possible to choose T_s such that the following approximation holds

$$A^2 \simeq \Psi_{H^d_{k,p,m}}[x(n)].$$

Letting $\Omega=2\pi\nu_0 T_s$, relation (39) gives

$$T_s = \frac{2k_1+1}{4(m-p)\nu_0} = \frac{1}{4\nu_0}, \tag{42}$$

where ν_0 is the carrier frequency. In white light interferometry, the mean wavelength is $\sim$640 nm for a carrier of $\nu_0=1/320\ \mathrm{nm}^{-1}$. Thus, T_s is equal to 80 nm. As an example of application the operators of orders $k=2$ and 4 are studied (see Section 4). These orders correspond to the following combinations of p, q, m, and l:

$$k=2 \quad \Rightarrow \quad p=2, \quad q=0, \quad m=1, \quad l=1,$$

$$k=4 \quad \Rightarrow \quad p=2, \quad q=2, \quad m=3, \quad l=1,$$

$$k=4 \quad \Rightarrow \quad p=3, \quad q=1, \quad m=4, \quad l=0.$$

The corresponding HEOs are designed by $\Psi_{H^d_{2,2,1}}$, $\Psi_{H^d_{4,2,3}}$, and $\Psi_{H^d_{4,3,4}}$, respectively. Note that $k=2$ corresponds to combinations $(p=2, q=0, m=1, l=1)$ and $(p=1, q=1, m=2, l=0)$ associated with the TKEO.

G. Comparison with the TKEO

Using Eq. (26) with the combination $(p=2, q=0, m=1, l=1)$ it is easy to verify that $\Psi_{H_{k,p,m}}$ is reduced to the TKEO:

$$\Psi_{H^d_{k,p,m}}[x(n)] = A^2\sin((2-1)\Omega)\sin((2+1-2)\Omega) = A^2\sin^2\Omega. \tag{43}$$

Relation (43) corresponds to the application of the TKEO to $x(n)$:

$$\Phi_2[x(n)] = x^2(n) - x(n-1)x(n+1). \tag{44}$$

Using combination $(p=1, q=1, m=2, l=0)$ with Eq. (10) we obtain

$$\Psi_{H^d_{k,p,m}}[x(n)] = \frac{1}{2}(x^2(n-1) + x^2(n+1) - x(n-2)x(n) - x(n+2)x(n)), \tag{45}$$

$$=\frac{1}{2}(\Phi_2[x(n-1)]+\Phi_2[x(n+1)]). \quad (46)$$

We find a propriety of the TKEO applied to a sinusoidal signal:

$$\Phi_2[x(n)]=\frac{\Phi_2[x(n-1)]+\Phi_2[x(n+1)]}{2}. \quad (47)$$

3. PARAMETERIZED HIGHER-ORDER ENERGY OPERATOR

As in [11] the HEO is generalized by introducing a lag parameter τ. This new class of operators is called parameterized HEO (PHEO). The PHEO, noted $\Psi_{PH_{k,\tau,p,m}}$, is defined as follows:

$$\begin{aligned}\Psi_{PH_{k,\tau,p,m}}[x(t)]=\frac{1}{2}[&x^{(p)}(t+\tau/2)x^{(q)}(t-\tau/2)\\&+x^{(p)}(t-\tau/2)x^{(q)}(t+\tau/2)\\&-(x^{(m)}(t+\tau/2)x^{(l)}(t-\tau/2)\\&+x^{(m)}(t-\tau/2)x^{(l)}(t+\tau/2))].\end{aligned}$$

Let $\gamma_{xy}(\tau;t)$ be the *instantaneous* cross correlation between $x(t)$ and $y(t)$:

$$\gamma_{xy}(\tau;t)=x\left(t-\frac{\tau}{2}\right)y\left(t+\frac{\tau}{2}\right).$$

Consider the transformation $\Phi_{PH_{k,\tau,p,m}}[x(t)]$, which associates to $x(t)$ the relation

$$\begin{aligned}\Phi_{PH_{k,\tau,p,m}}[x(t)]=&\gamma_{x^{(p)}x^{(q)}}(\tau;t)+\gamma_{x^{(p)}x^{(q)}}(-\tau;t)\\&-\gamma_{x^{(m)}x^{(n)}}(\tau;t)-\gamma_{x^{(m)}x^{(n)}}(-\tau;t), \quad (48)\end{aligned}$$

where $m+n=p+q$. Thus, $\Phi_{PH_{k,\tau,p,m}}$ may be viewed as PHEO applied to random processes. In this work we limit ourselves to deterministic signals. Thus, $\Phi_{PH_{k,\tau,p,m}}$ is reduced to $\Psi_{PH_{k,\tau,p,m}}$. For $\tau=0$ and appropriate combinations of the orders (p,q,m,l), the operators TKEO, DEO, and HEO can easily be deduced from the PHEO. Using the reasoning with the same assumptions as for the HEO, the $\Psi_{PH_{k,\tau,p,m}}$ outputs for $x(t_0)$ and $\dot{x}(t_0)$ are given by

$$\Psi_{PH_{k,\tau,p,m}}[x(t_0)]=A^2\Omega_\tau^k\cos(\Omega_\tau\tau)\sin\left(\frac{\pi}{4}c\right)\sin\left(\frac{\pi}{4}b\right),$$

$$\Psi_{PH_{k,\tau,p,m}}[\dot{x}(t_0)]=A^2\Omega_\tau^{k+2}\cos(\Omega_\tau\tau)\sin\left(\frac{\pi}{4}c\right)\sin\left(\frac{\pi}{4}b\right).$$

Note that for each lag, τ, corresponds an IF, Ω_τ. Provided that $\cos(\Omega_\tau\tau)\sin[(\pi/4)c]\sin[(\pi/4)b]\neq 0$, in the same manner as in Subsection 2.B, one can write

$$\begin{aligned}\frac{\Psi_{PH_{k,\tau,p,m}}[\dot{x}(t_0)]}{\Psi_{PH_{k,\tau,p,m}}[x(t_0)]}&=\frac{A^2\omega_\tau^{k+2}\cos(\Omega_\tau\tau)\sin[(\pi/4)c]\sin[(\pi/4)b]}{A^2\Omega_\tau^k\cos(\Omega_\tau\tau)\sin[(\pi/4)c]\sin[(\pi/4)b]},\\&=\Omega_\tau^2, \quad (49)\end{aligned}$$

$$\begin{aligned}\frac{\Psi^2_{PH_{k,\tau,p,m}}[x(t_0)]}{\Psi_{PH_{2k,\tau,p1,m1}}[x(t_0)]}&=\frac{A^4\Omega_\tau^{2k}\cos^2(\Omega_\tau\tau)\sin^2[(\pi/4)c]\sin^2[(\pi/4)b]}{A^2\Omega_\tau^{2k}\cos(\Omega_\tau\tau)\sin[(\pi/4)c_1]\sin[(\pi/4)b_1]}\\&=A^2\cos(\Omega_\tau\tau)\frac{\sin^2[(\pi/4)c]\sin^2[(\pi/4)b]}{\sin[(\pi/4)c_1]\sin[(\pi/4)b_1]}. \quad (50)\end{aligned}$$

Under the assumption $|\cos(\Omega_\tau\tau)|=1$, it is possible to demodulate an AM-FM signal. When τ takes its values in a local interval around t_0, we have the property of periodicity:

$$\tau=\frac{n\pi}{2\Omega_\tau}, \quad n \text{ integer} \quad \Rightarrow \quad \Psi_{PH_{k,\tau,p,m}}=\Psi_{PH_{k,0}}. \quad (51)$$

Consequently, for a given even order, we are able to find, in theory, many operators to extract locally the envelope and the IF of an AM-FM signal. However, condition (51) supposes that the IF is known before applying our operators. As for the HEO, A_τ and Ω_τ are estimated in each short interval $J\subset T$ to have an estimation of the envelope and the IF, over the interval T, of $x(t)$. Again under the assumptions $|\sin(a\pi/4)\sin(b\pi/4)|\simeq 1$ and $|\cos(\Omega_\tau\tau)|\neq 0$ we deduce

$$\omega_\tau^2(t)\simeq\frac{\Psi_{PH_{k,\tau,p,m}}[\dot{x}(t)]}{\Psi_{PH_{k,\tau,p,m}}[x(t)]}, \quad (52)$$

$$\hat{a}_\tau^2(t)\simeq\frac{1}{|\cos(\omega_\tau(t)\tau)|}\frac{\Psi^2_{PH_{k,\tau,p,m}}[x(t)]}{|\Psi_{PH_{2k,\tau,p1,m1}}[x(t)]|}. \quad (53)$$

Thus, it is possible to extract the envelope and above all, the IF independently of the current parameter τ. It is expected that the estimation of instantaneous envelope be sensitive for very noisy data. Moreover, even the proposed solution takes theoretically into account the neighborhood of each sample for any τ, it is also expected that the estimation can be biased for very high τ value.

A possible solution to this problem is to oversample the processed signal and then average the estimated amplitudes and/or frequencies. To improve the robustness, we propose to average $\omega_\tau(t)$ for different τ values:

$$\hat{\omega}(t)=\frac{1}{T}\int_0^T\omega_\tau(t)\mathrm{d}\tau. \quad (54)$$

Using $\hat{\omega}(t)$ we re-estimate the envelope [Eq. (53)]. Identically, the estimated envelopes are averaged as

$$\widehat{a(t)}=\frac{1}{T}\int_0^T\hat{a}_\tau(t)\mathrm{d}\tau. \quad (55)$$

For oversampled data, we set $T\simeq$ to $1/d$, where d is the oversampling factor. The same approach can also be applied for the nonparameterized methods by averaging the estimated values inside a window of size d. The oversampled parameterized and nonparameterized algorithms are called, respectively, OS-PHEO and OS-HEO.

4. RESULTS

Results of envelope and frequency detections by the proposed energy operators are illustrated on synthetic and real signals. For synthetic signal, detection is performed on clean and noisy (ratio standard deviation–amplitude of 2% and 4%) signals. We focus our attention on the case of an AM signal that is a sinusoid modulated by a damped exponential. We compare the discrete operators $\Psi_{H^d_{k,p,m}}$ [Eq. (10)] with those of Maragos and Potamianos [7].

A. Discrete Operators

1. Real Interferometric Signal

Figure 1(a) represents a real image obtained by an interference microscopy system [12]. This image corresponds to a sequence of scanned images of a slanted step of silicon, along the x-depth–rows axis. The peak of the fringe envelope along the vertical axis gives the position of the air–layer surface. The real image corresponds to $T_s = 10$ nm. These real data are downsampled by a factor of 4 to be compatible with condition (42). A general approximation of the intensity along the vertical axis is the AM signal $x(t)$ as shown in Fig. 1(b). For such an image an average wavelength of 640 nm in white light scanning interferometry system corresponds to a vertical oriented modulated frequency $\nu_0 = 1/320\ \text{nm}^{-1}$. Different signal processing techniques used in coherence probe microscopy, also known as white light scanning interference microscopy, for measurement of surface roughness have been proposed [13]. Most of the methods are based on the AM modulated signal model, which represents the variation in light intensity measured along the optical axis of an interference microscope. Larkin demodulates such signals column-by-column using the well-known five sample algorithm (FSA) [14], which performs the 1D discrete TKEO along the x axis but applied to the differentiated version of the signal. The profile given by Fig. 1(c) may be seen as the ground truth. Results of demodulation by $\Psi_{H^d_{k,p,m}}$ and Φ_{km} are shown in Figs. 2 and 3, respectively. To compare quantitatively the results of the operators, maximum and mean values of error of envelope estimation are summarized in Table 1. Error is measured between the estimated envelope and the reference profile. Quantitatively the best results are given by $\Psi_{H^d_{4,2,3}}$ [Fig. 2(a)] and Φ_{01} [Fig. 3(a)]. This result is confirmed by a low envelope mean error of 2 nm (Table 1). Note that $\Psi_{H^d_{4,2,3}}$ is slightly better than Φ_{01} with a low maximum error of 12.64 nm.

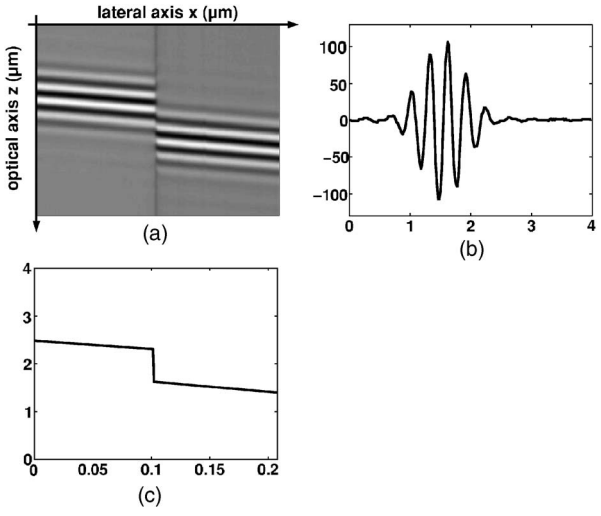

Fig. 1. (a) Interferometric signal, (b) a profile along the optical axis, and (c) the reference surface shape.

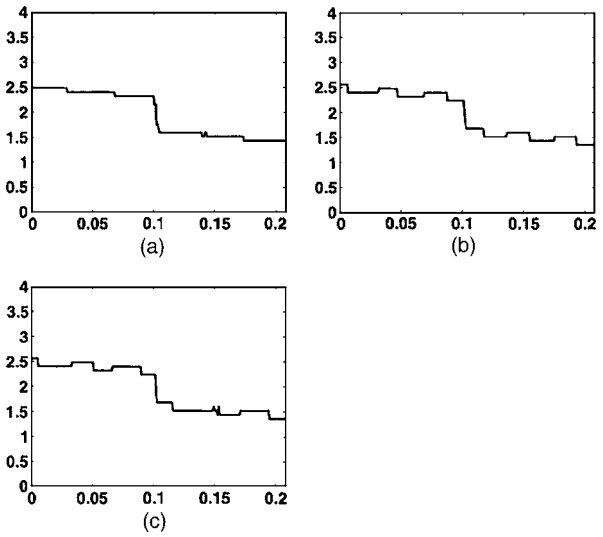

Fig. 2. Envelope detection of real signal by $\Psi_{H^d_{k,p,m}}$, (a) $\Psi_{H^d_{4,2,3}}$, (b) $\Psi_{H^d_{4,3,4}}$, (c) $\Psi_{H^d_{2,2,1}}$.

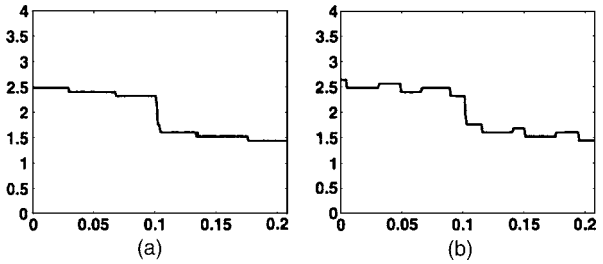

Fig. 3. Envelope detection of real signal by Φ_{km}, (a) Φ_{01}, (b) Φ_{21}.

Table 1. Quantitative Results of Envelope Detection of Real Signal Using $\Psi_{H^d_{k,p,m}}$ and Φ_{km} Operators

Operators	Mean Error (nm)	Max Error (nm)
$\Psi_{H^d_{2,2,1}}$	5.76	21.49
$\Psi_{H^d_{4,2,3}}$	2.00	12.64
$\Psi_{H^d_{4,3,4}}$	6.00	19.54
Φ_{01}	2.00	12.95
Φ_{21}	6.20	20.71

2. Synthetic Signal

An example of such a signal with a carrier frequency of 5 Hz and its noisy version are shown in Figs. 4(a) and 4(d), respectively. The envelope and the carrier frequency are shown in Figs. 4(b) and 4(c), respectively. Results of envelope detection by $\Psi_{H^d_{k,p,m}}$ and Φ_{km} are shown in Figs. 5 and 6, respectively. Visual inspection of the resulting envelopes (Figs. 5 and 6) shows that results of $\Psi_{H^d_{k,p,m}}$ are comparable with those of Φ_{km} (Table 2). In terms of mean error, globally, $\Psi_{H^d_{k,p,m}}$ performs better than Φ_{km}. Results

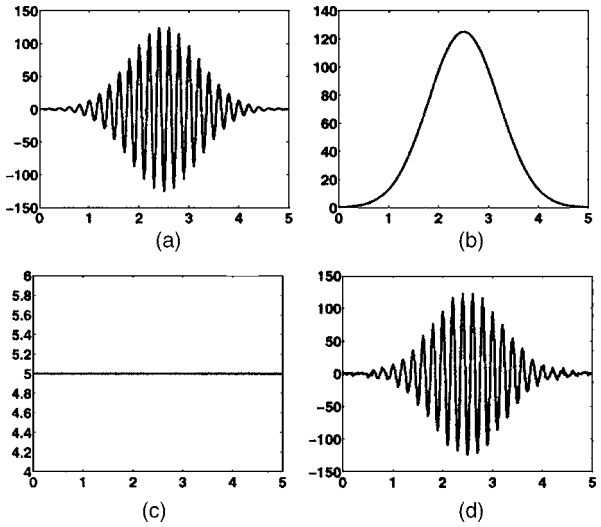

Fig. 4. (a) Original AM signal, (b) its envelope, (c) related frequency, and (d) noisy signal.

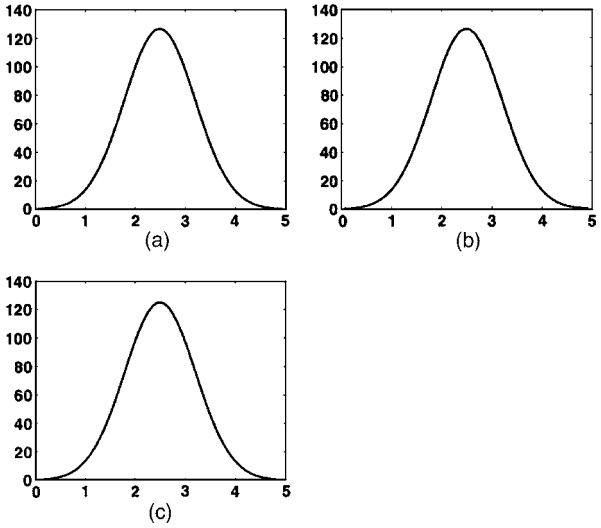

Fig. 5. Envelope detection of synthetic signal by $\Psi_{H^d_{k,p,m}}$, (a) $\Psi_{H^d_{2,2,1}}$, (b) $\Psi_{H^d_{4,2,3}}$, (c) $\Psi_{H^d_{4,3,4}}$.

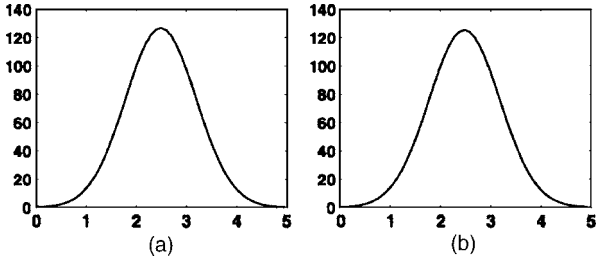

Fig. 6. Envelope detection of synthetic signal by Φ_{km}, (a) Φ_{01}, (b) Φ_{21}.

Table 2. Quantitative Results of Envelope Detection of Synthetic Signal Using $\Psi_{H^d_{k,p,m}}$ and Φ_{km} Operators

Operators	$\Psi_{H^d_{2,2,1}}$	$\Psi_{H^d_{4,2,3}}$	$\Psi_{H^d_{4,3,4}}$	Φ_{01}	Φ_{21}
Mean error (%)	4.1	4.9	4.74	4.17	7.03

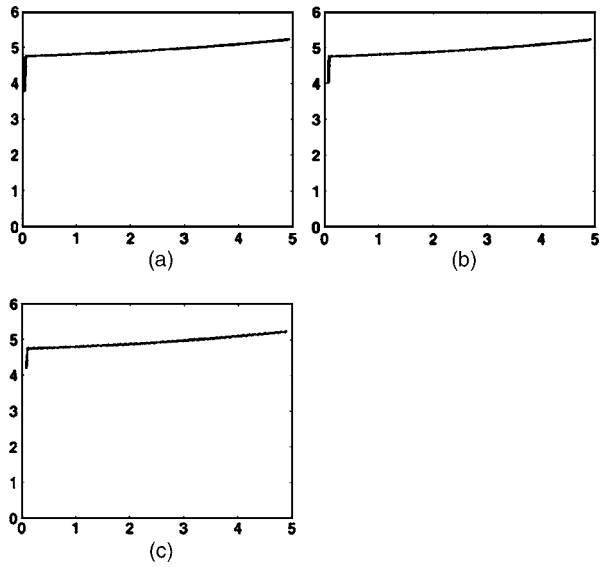

Fig. 7. Frequency detection of synthetic signal by $\Psi_{H^d_{k,p,m}}$, (a) $\Psi_{H^d_{2,2,1}}$, (b) $\Psi_{H^d_{4,2,3}}$, (c) $\Psi_{H^d_{4,3,4}}$.

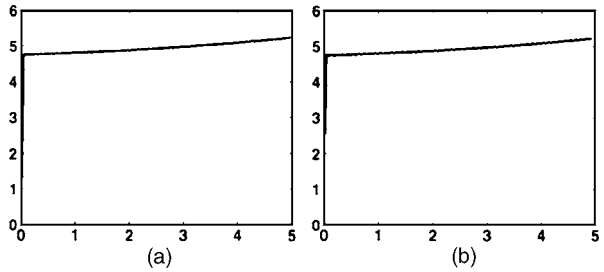

Fig. 8. Frequency detection of synthetic signal by Φ_{km}, (a) Φ_{01}, (b) Φ_{21}.

Table 3. Quantitative Results of Frequency Detection of Synthetic Signal Using $\Psi_{H^d_{k,p,m}}$ and Φ_{km} Operators

Operators	$\Psi_{H^d_{2,2,1}}$	$\Psi_{H^d_{4,2,3}}$	$\Psi_{H^d_{4,3,4}}$	Φ_{01}	Φ_{21}
Mean error (%)	4.3	5	5.77	3.73	4.43

of frequency detection by $\Psi_{H^d_{k,p,m}}$ and Φ_{km} are shown in Figs. 7 and 8, respectively. Even Φ_{km} gives better results in terms of mean error (Table 3); $\Psi_{H^d_{k,p,m}}$ introduces less ringing effect (Fig. 7) than Φ_{km} (Fig. 8).

B. Continuous Operators

1. Synthetic Signal

Results of envelope detection by HEO, OS-HEO, PHEO, and OS-PHEO are compared. Note that for the chosen k values, the HEO and the classic continuous Teager–Kaiser are identical. For OS-HEO ($d>1$), the signal of T duration is oversampled by a factor d, and $T\times d$ envelopes, $a(n)$, and IFs, $\omega(n)$ values are estimated. Each estimated frequency or envelope is averaged over a window of size d to finally obtain T values. Figures 9(a) and 9(b) show the result given by the HEO using, respectively, the functions $(\Psi_{H_{2,2,1}},\Psi_{H_{4,2,3}})$ and $(\Psi_{H_{4,2,3}},\Psi_{H_{8,4,5}})$ using non-over-sampled data ($d=1$). We note that the envelope amplitude is underestimated by the HEO. Figures

10(a)–10(d) show the result of the HEO approach for $k=(2,4)$ and $k=(4,8)$ using an oversampling factor, respectively, of $d=5$ and 10. The envelope amplitude is not underestimated. This result shows a link between the oversampling and the estimation: the oversampled signal is naturally close to the continuous one. However, due to successive derivatives, the lower the order k, the better the estimation. Actually, for parameters $k=(4,8)$ the combination of the higher-order derivative value, the oversampling, and the spline functions provide some ripples around the maximum of the envelope [Fig. 10(d)]. In the same way, we note for PHEO an underestimation of the amplitude without oversampling [Figs. 11(a) and 11(b)]; and a corrected level provided by oversampled data, respectively, with $d=5$ and 10 [Figs. 12(a)–12(d)]. A careful examination of the detected envelopes shown in Figs. 10(a), 10(b), 13(a), and 13(b), and the original envelope [Fig. 4(b)] shows that the OS-HEO and the HEO give the same result for an oversampling factor $d=5$. Figures 13(a) and 13(b) show the detection envelope using the OS-HEO method for $k=(2,4)$ and $(4,8)$. The τ parameter takes its values in the range $[-T,T]$ with $T=5$. A careful examination of the detected envelopes shown in Figs. 12(a), 12(b), 14(a), and 14(b), and the original envelope [Fig. 4(b)] shows that the OS-PHEO and the PHEO have the same behavior for an oversampling factor $d=5$. These results are confirmed by the error rates reported in Table 4. This table compares the error rate of the HEO, PHEO, OS-HEO, OS-PHEO, and the Hilbert transform for two different window sizes (applying the OS-PHEO). The rates decrease with the oversampling. The error rate provided by the PHEO method for $d=1$ (33.21%) versus $d=5$ (3.40%) confirms the previous assumptions. One can notice that the OS-PHEO provides the best results without oversam-

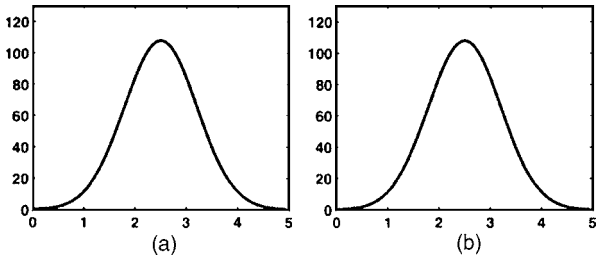

Fig. 9. Envelope detection of synthetic signal with an oversampling factor $d=1$ using (a) HEO, $k=(2,4)$; (b) HEO, $k=(4,8)$.

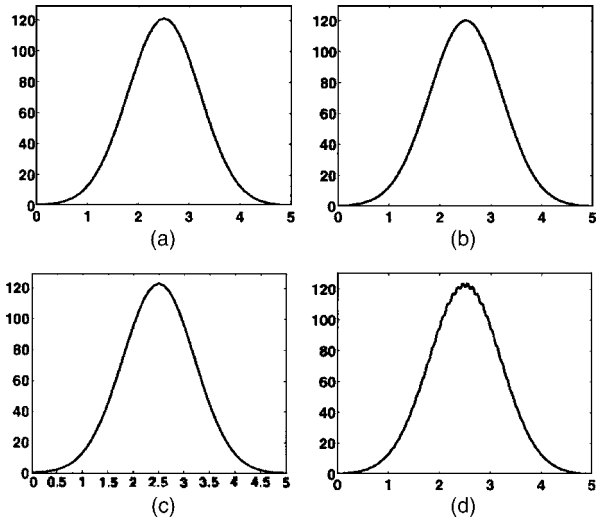

Fig. 10. Envelope detection with an oversampling factor $d=5$: (a) HEO, $k=(2,4)$; (b) HEO, $k=(4,8)$; $d=10$: (c) HEO, $k=(2,4)$; (d) HEO, $k=(4,8)$.

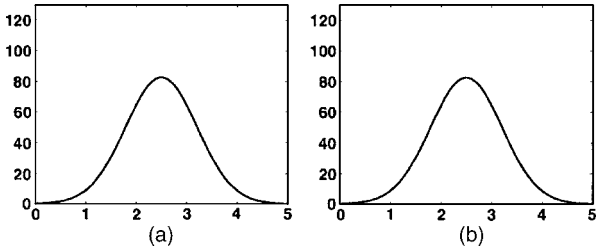

Fig. 11. Envelope detection of synthetic signal with an oversampling factor $d=1$ using (a) PHEO, $k=(2,4)$; (b) PHEO, $k=(4,8)$.

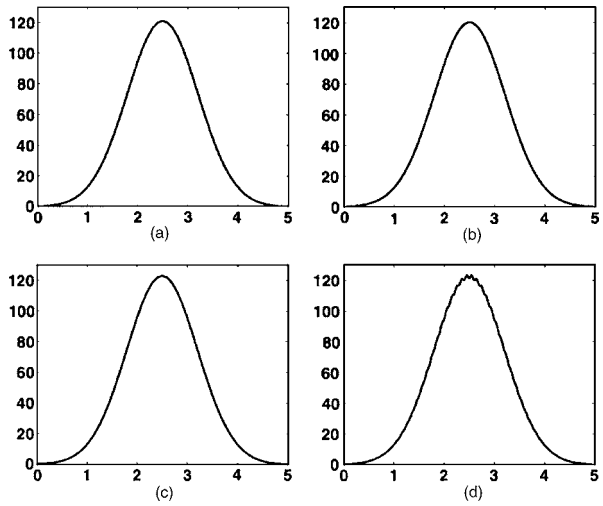

Fig. 12. Envelope detection with an oversampling factor $d=5$: (a) PHEO, $k=(2,4)$; (b) PHEO, $k=(4,8)$; $d=10$: (c) PHEO, $k=(2,4)$; (d) PHEO, $k=(4,8)$.

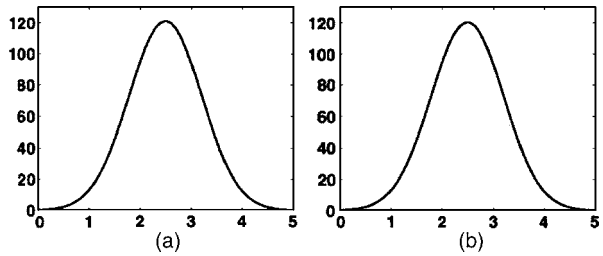

Fig. 13. Envelope detection of synthetic signal with an oversampling factor $d=5$ using (a) OS-HEO, $k=(2,4)$; (b) OS-HEO, $k=(4,8)$.

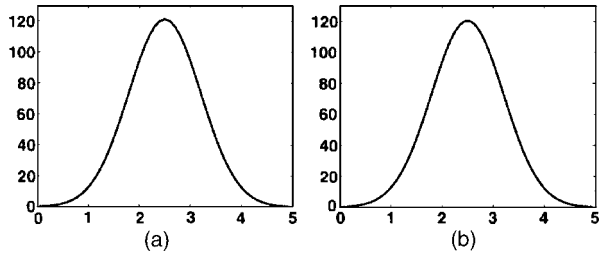

Fig. 14. Envelope detection of synthetic signal with an oversampling factor $d=5$ using (a) OS-PHEO, $k=(2,4)$; (b) OS-PHEO, $k=(4,8)$.

Table 4. Nonnoisy Envelope Estimation: Error Rate (%) for $k=(2,4)$ with Different Oversampling Factors d and Window Sizes

Operator Type	$d=1$; $T=5$ (%)	$d=1$; $T=10$ (%)	$d=5$; $T=5$ (%)	$d=5$; $T=10$ (%)
HEO	13.27	13.27	3.40	3.40
PHEO ($\tau=1$)	33.21	33.21	3.40	3.40
OS-HEO	13.27	13.27	3.39	3.39
OS-PHEO	**9.86**[a]	**8.22**	3.39	3.46
Hilbert	13.24	13.24	2.98	2.98

[a]Boldface denotes minimum values of error rates.

Table 5. Noisy Envelope Estimation: Error rate (%) for $k=(2,4)$; Oversampling Factor $d=1$

Operator Type	Noise=2%; $T=5$ (%)	Noise=2%; $T=10$ (%)	Noise=4%; $T=5$ (%)	Noise=4%; $T=10$ (%)
HEO	15.59	15.59	19.37	19.37
PHEO ($\tau=1$)	33.46	33.46	35.10	35.10
OS-HEO	15.59	15.59	19.37	19.37
OS-PHEO	**12.44**[a]	**11.82**	**16.69**	**17.06**
Hilbert	15.17	15.17	19.90	19.90

[a]Boldface denotes minimum values of error rates.

Table 6. Noisy Envelope Estimation: Error Rate (%) for $k=(2,4)$, Oversampling Factor $d=5$

Operator Type	Noise=2%; $T=5$ (%)	Noise=2%; $T=10$ (%)	Noise=4%; $T=5$ (%)	Noise=4%; $T=10$ (%)
HEO	14.36	14.36	20.31	20.31
PHEO ($\tau=1$)	13.94	13.94	19.86	19.86
OS-HEO	**13.59**[a]	**13.59**	**19.13**	**19.13**
OS-PHEO	13.67	14.60	19.68	21
Hilbert	11.50	11.50	17.22	17.22

[a]Boldface denotes minimum values of error rates.

pling (first two columns of Table 4). The synthetic signal is then contaminated by an additive noise of intensity 2% and 4%. We summarized the quantitative results of the envelope detection in Table 5, for two sampling factors ($d=1$ and 5), two noise levels, and two window sizes of T (the window associated to the PHEO). The results are performed averaging 200 simulations. We compared the previous operators with the Hilbert approach. For non-over-sampled data, the OS-PHEO is competitive versus the other methods in both noisy and nonnoisy environments. The presented results for the nonnoisy data are confirmed by the HEO, PHEO, and OS-PHEO: the oversampling improves the error rates particularly for the PHEO method. We note an exception for the OS-PHEO, which is less competitive for $d=5$. More generally the OS-HEO and OS-PHEO are more robust than the other nonlinear approaches. However, the Hilbert approach still remains competitive for the oversampled factor $d=5$ for noisy data (Table 6).

Frequency detection using, respectively, $\Psi_{H_{2,2,1}}$ and $\Psi_{H_{4,2,3}}$ [Eq. (22)] is shown in Figs. 15(a) and 15(b). Again for HEO, the estimation has been improved by an oversampling of the data (see Fig. 16). Figures 17 and 18 show the estimated frequency of the oversampled signal by factor of $d=5$ using the OS-HEO and OS-PHEO, respectively. In the same way, the oversampled data [see Figs. 19(a), 19(b), and 20] improves the estimation in the parameterized case (PHEO). The oversampling of the data improves the frequency estimation in both the noisy and nonnoisy contexts with the low noise (see Tables 7–9). For a higher noise level (4%) the rates improve when $T=5$ and $d=5$, but the difference is less significant. Concerning the frequency estimation, all nonlinear methods provide nearly comparative results, specifically the PHEO method in the non-over-sampled context: actually we have shown

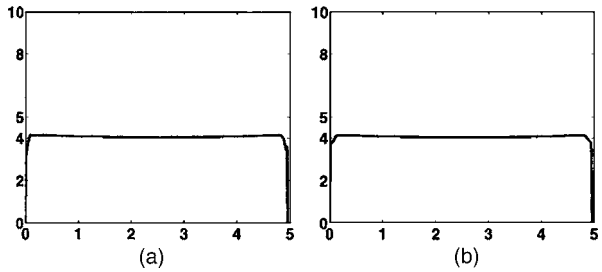

Fig. 15. Frequency detection of synthetic signal with an oversampling factor $d=1$ using (a) HEO, $k=(2,4)$; (b) HEO, $k=(4,8)$.

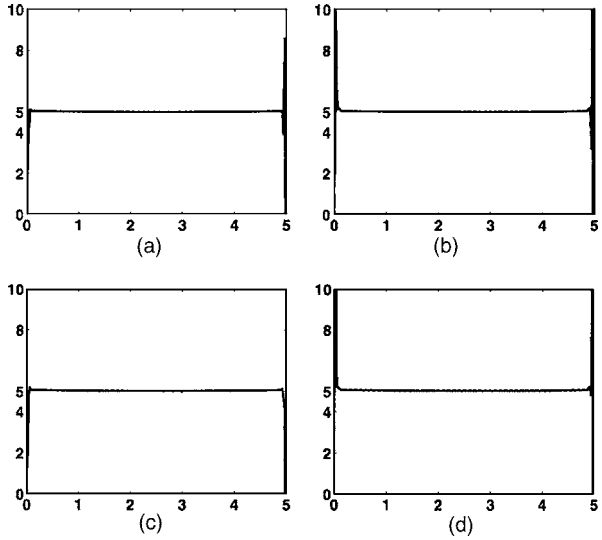

Fig. 16. Frequency detection with an oversampling factor $d=5$: (a) HEO, $k=(2,4)$; (b) HEO, $k=(4,8)$; $d=10$: (c) HEO, $k=(2,4)$; (d) HEO, $k=(4,8)$.

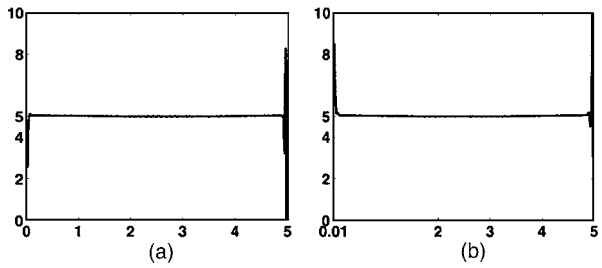

Fig. 17. Frequency detection of synthetic signal with an oversampling factor $d=5$ using (a) OS-HEO, $k=(2,4)$; (b) OS-HEO, $k=(4,8)$.

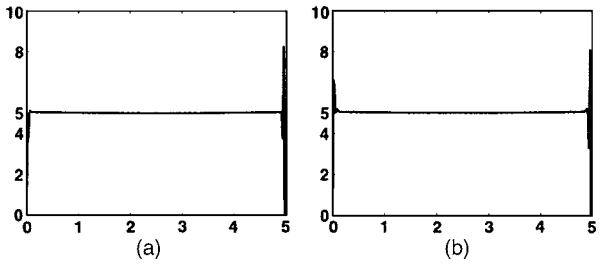

Fig. 18. Frequency detection of synthetic signal with an oversampling factor $d=5$ using (a) OS-PHEO, $k=(2,4)$; (b) OS-PHEO, $k=(4,8)$.

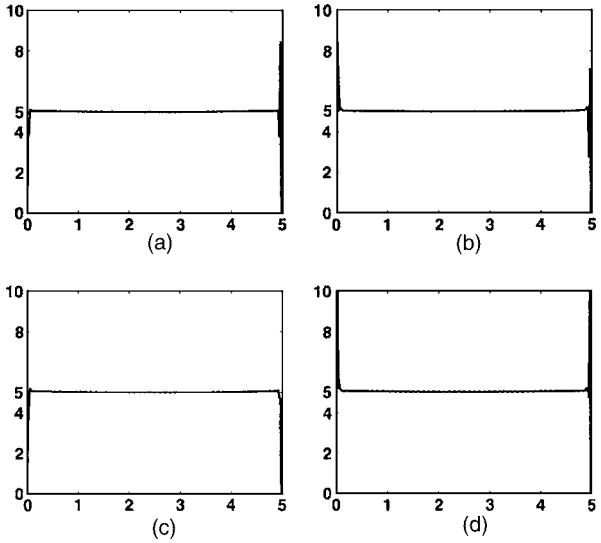

Fig. 19. Frequency detection with an oversampling factor $d=5$: (a) PHEO, $k=(2,4)$; (b) PHEO, $k=(4,8)$; $d=10$: (c) PHEO, $k=(2,4)$; (d) PHEO, $k=(4,8)$.

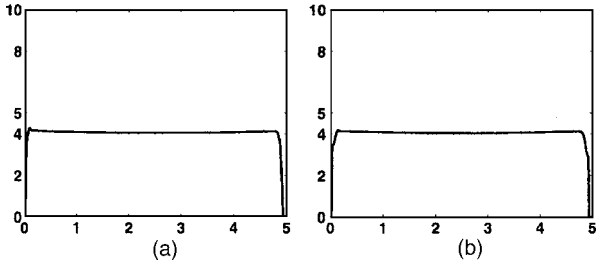

Fig. 20. Frequency detection of synthetic signal with an oversampling factor $d=1$ using (a) PHEO, $k=(2,4)$; (b) PHEO, $k=(4,8)$.

previously that the IF is extracted independently of the parameter τ.

2. Real Interferometric Signal

The resulting profiles and the corresponding error rates ε are summarized in Fig. 21 for $k=(2,4)$. Even the HEO gives good results; the best error rates are given by the OS-HEO and the OS-PHEO. This suggests that the postover-sampling approach is an interesting way to perform such surface detection. Note that the worst results are given by the PHEO.

5. CONCLUSION

In this paper a new nonlinear high-order operator class called the higher-order energy operator (HEO), which is an extension of the TKEO and the DEO, is presented. A unified version of the HEO, corresponding to a class of continuous parameterized operators, called PHEO, is also

Table 7. Nonnoisy Frequency Estimation: Error Rate (%) for $k=(2,4)$ with Different Oversampling Factors and Windows

Operator Type	$d=1$; $T=5$ (%)	$d=1$; $T=10$ (%)	$d=5$; $T=5$ (%)	$d=5$; $T=10$ (%)
HEO	18.68	18.68	0.24	0.24
PHEO ($\tau=1$)	18.79	18.79	0.24	0.24
OS-HEO	18.68	18.68	0.24	0.24
OS-PHEO	18.71	18.63	0.24	0.24

Table 8. Noisy Frequency Estimation: Error Rate for $k=(2,4)$; Oversampling Factor $d=1$

Operator Type	Noise=2%; $T=5$ (%)	Noise=2%; $T=10$ (%)	Noise=4%; $T=5$ (%)	Noise=4%; $T=10$ (%)
HEO	**18.92**[a]	18.92	**20.02**	20.02
PHEO ($\tau=1$)	20.48	20.48	23.10	23.10
OS-HEO	**18.92**	18.92	**20.02**	20.02
OS-PHEO	19.02	**18.60**	20.15	**19.15**

[a]Boldface denotes minimum values of error rates.

Table 9. Noisy Frequency Estimation: Error Rate for $k=(2,4)$; Oversampling Factor $d=5$

Operator Type	Noise=2%; $T=5$ (%)	Noise=2%; $T=10$ (%)	Noise=4%; $T=5$ (%)	Noise=4%; $T=10$ (%)
HEO	11.33	11.33	19.03	**19.03**[a]
PHEO ($\tau=1$)	11.53	11.53	20.42	20.42
OS-HEO	10.58	**10.58**	19.07	19.07
OS-PHEO	**10.22**	11.34	**17.46**	21.54

[a]Boldface denotes minimum values of error rates.

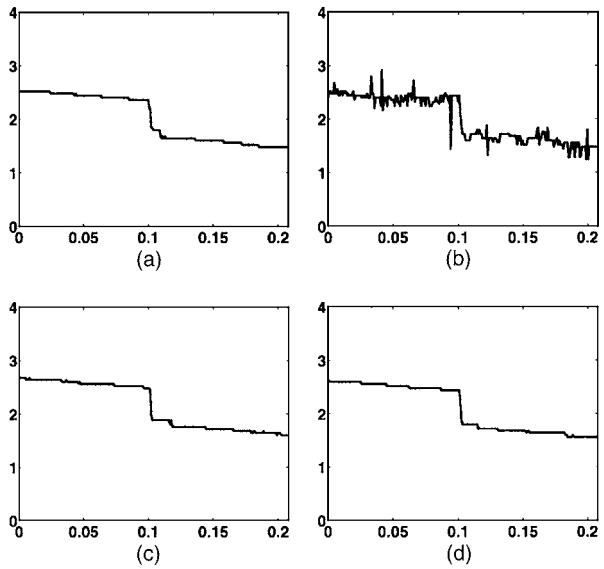

Fig. 21. Surface detection using (a) HEO, $k=(2,4)$; $\varepsilon=17.3$ nm; (b) PHEO, $k=(2,4)$; $\varepsilon=70.2$ nm; (c) OS-HEO, $k=(2,4)$; $\varepsilon=16.3$ nm; (d) OS-PHEO, $k=(2,4)$; $\varepsilon=15.3$ nm.

introduced. When the derivative order is an even integer, it is possible to demodulate an AM-FM signal, provided that the partial derivatives satisfy certain conditions. One main advantage of the methods presented is the choice of the derivative order, which is flexible: choosing a given order, the operator proposed by Maragos and Potamianos [7] provides only one solution: the order corresponds to the order of the derivative. In our case, the order of the derivatives are lower than the order of the operator. Results of PHEO and OS-PHEO showed that the estimated instantaneous frequency is locally independent of the lag parameter. Results on AM signal detection show that envelopes are better detected by OS-HEO and OS-PHEO than HEO and PHEO. The oversampling of data yields encouraging results for all methods. These operators are also used to estimate the envelope and the instantaneous frequency for surface roughness detection used in interferometry. In parallel, we developed discrete solutions that appear competitive facing the classic discrete approaches. In future work, we plan to extend the proposed operators to image processing to estimate local amplitude and frequency for image segmentation purposes.

REFERENCES

1. J. F. Kaiser, "Some useful properties of Teager's energy operator," in *Proceedings of IEEE International Conference on Acoustics, Speech, and Signal Processing* (IEEE, 1993), pp. 149–152.
2. P. Maragos, T. F. Quatieri, and J. F. Kaiser, "Energy separation in signal modulations with applications to speech analysis," IEEE Trans. Signal Process. **41**, 3024–3051 (1993).
3. F. Salzenstein, P. C. Montgomery, D. Montaner, and A. O. Boudraa, "Teager–Kaiser energy and higher-order operators in white-light interference microscopy for surface shape measurement," J. App. Sig. Proc. **17**, 2804–2815 (2005).
4. P. Maragos and A. Bovik, "Image demodulation using multidimensional energy separation," J. Opt. Soc. Am. A **12**, 1867–1876 (1995).
5. F. Salzenstein, P. Montgomery, A. Benatmane, and A. O. Boudraa, "2D discrete high order energy operators for surface profiling using white light interferometry," in *Proceedings of International Symposium on Signal Processing and its Applications* (IEEE, 2003), pp. 601–604.
6. B. Santhanam and P. Maragos, "Energy demodulation of two component AM-FM signals with application to speaker separation," in *Proceedings of IEEE International Conference on Acoustics, Speech, and Signal Processing* (IEEE, 1996), p. 3518.
7. P. Maragos and A. Potamianos, "Higher-order differential energy operators," IEEE Signal Process. Lett. **2**, 152–154 (1995).
8. A. O. Boudraa, F. Salzenstein, and J. C. Cexus, "Two-dimensional continuous higher-order energy operators," Opt. Eng. (Bellingham) **44**, 7001–7009 (2005).
9. A. Potamianos and P. Maragos, "A comparison of the energy operator and the Hilbert transform approach to signal and speech demodulation," Signal Process. **37**, 95–120 (1994).
10. P. Flandrin, *Temps-Fréquence* (Hermès, 1998).
11. L. Wei, C. Hamilton, and P. Chitrapu, "A generalization to the Teager–Kaiser energy function and application to resolving two closely-spaced tones," in *Proceedings of IEEE International Conference on Acoustics, Speech, and Signal Processing* (IEEE, 1995), p. 1637.
12. P. C. Mongomery, A. Benatmane, E. Fogarassy, and J. P. Ponpon, "Large area, high resolution analysis of surface roughness of semiconductors using interference microscopy," Mater. Sci. Eng. B **91–92**, 79–82 (2002).
13. S. S. Chim and G. S. Kino, "Correlation microscope," Opt. Lett. **15**, 579–581 (1990).
14. K. G. Larkin, "Efficient nonlinear algorithm for envelope detection in white light interferometry," J. Opt. Soc. Am. A **13**, 832–843 (1996).